Available online at www.sciencedirect.com
ScienceDirect
Biochimica et Biophysica Acta 1758 (2006) 948–959
BIOCHIMICA ET BIOPHYSICA ACTA
BBA
www.elsevier.com/locate/bbamem

Review

FTIR-microspectroscopy of prion-infected nervous tissue

Ariane Kretlow [a], Qi Wang [b], Janina Kneipp [c], Peter Lasch [a], Michael Beekes [d], Lisa Miller [b], Dieter Naumann [a,*]

[a] *P25, Robert Koch-Institut, Nordufer 20, 13353 Berlin, Germany*
[b] *NSLS, Brookhaven National Laboratory, Upton, NY, USA*
[c] *Federal Institute for Materials Research and Testing, FG I.3, Richard-Willstätter-Str. 11, 12489 Berlin, Germany*
[d] *P24, Robert Koch-Institut, Nordufer 20, 13353 Berlin, Germany*

Received 15 March 2006; received in revised form 4 May 2006; accepted 8 May 2006
Available online 7 June 2006

Abstract

The family of transmissible spongiform encephalopathies (TSE), also termed prion diseases, is a group of fatal, neurodegenerative diseases characterized by the accumulation of a misfolded protein, the disease-associated prion protein PrP^{Sc}. This glycoprotein differs in secondary structure from its normal, cellular isoform PrP^{C}, which is physiologically expressed mostly by neurons. Scrapie is a prion disease first described in the 18th century in sheep and goats, and has been established as a model in rodents to study the pathogenesis and pathology of prion diseases. Assuming a multitude of molecular parameters change in the tissue in the course of the disease, FTIR microspectroscopy has been proposed as a valuable new method to study and identify prion-affected tissues due to its ability to detect a variety of changes in molecular structure and composition simultaneously. This paper reviews and discusses results from previous FTIR microspectroscopic studies on nervous tissue of scrapie-infected hamsters in the context of histological and molecular alterations known from conventional pathogenesis studies. In particular, data from studies reporting on disease-specific changes of protein structure characteristics, and also results of a recent study on hamster dorsal root ganglia (DRG) are discussed. These data include an illustration on how the application of a brilliant IR synchrotron light source enables the in situ investigation of localized changes in protein structure and composition in nervous cells or tissue due to PrP^{Sc} deposition, and a demonstration on how the IR spectral information can be correlated with results of complementary studies using immunohistochemistry and x-ray fluorescence techniques. Using IR microspectroscopy, some neurons exhibited a high accumulation of disease-associated prion protein evidenced by an increased amount of β-sheet at narrow regions in or around the infected nervous cells. However, not all neurons from terminally diseased hamsters showed PrP^{Sc} deposition. Generally, the average spectral differences between all control and diseased DRG spectra are small but consistent as demonstrated by independent experiments. Along with studies on the purified misfolded prion protein, these data suggest that synchrotron FTIR microspectroscopy is capable of detecting the misfolded prion protein in situ without the necessity of immunostaining or purification procedures. Published by Elsevier B.V.

Keywords: Scrapie; PrP^{Sc}; PrP^{C}; Synchrotron infrared microspectroscopy; Dorsal root ganglia; Chemical mapping

Contents

1. Introduction . . . 949
1.1. Scrapie and other transmissible spongiform encephalopathies . . . 949
1.2. Prions: structure, function and the prion hypothesis . . . 949
1.3. The scrapie 263K hamster model . . . 950
1.4. FTIR microspectroscopy of biological tissue . . . 950

* Corresponding author. Tel.: +49 30 45472259; fax: +49 30 45472606.
E-mail addresses: KretlowA@rki.de (A. Kretlow), NaumannD@rki.de (D. Naumann).

0005-2736/$ - see front matter. Published by Elsevier B.V.
doi:10.1016/j.bbamem.2006.05.026

2. Methods and approaches for studying scrapie-infected tissue by FTIR microspectroscopy . . . 951
2.1. Animal experiments and sample preparation . . . 951
2.2. Conventional IR spectroscopic studies of brain tissue from scrapie infected hamsters . . . 951
2.3. Synchrotron FTIR imaging of dorsal root ganglion tissue of scrapie . . . 952
2.4. Different spectroscopic regions analyzed in the scrapie studies . . . 952
3. FTIR-based detection of pathological changes in scrapie-infected hamsters . . . 952
4. FTIR microspectroscopy of dorsal root ganglia utilizing a synchrotron IR light source . . . 957
5. Concluding remarks and outlook . . . 957
Acknowledgements . . . 958
References . . . 958

1. Introduction

1.1. Scrapie and other transmissible spongiform encephalopathies

Scrapie is a neurodegenerative disorder of the central nervous system characterized by the accumulation of a β-sheet rich protein, the "Scrapie amyloid", and has been first described 1732 in sheep. The name "Scrapie" was derived from the observation that due to intense itchiness the animals scrape off their coat. Other symptoms include jumpiness, excessive loss of weight, tremor, loss of coordination and behavioral changes. A unique feature of the family of Transmissible Spongiform Encephalopathies (TSE), to which Scrapie belongs, is the fact that they can occur sporadically but may also have genetic and infectious origins. Transmissibility of Scrapie was first shown experimentally in 1960, when Chandler succeeded in transmitting the disease to mice [1]. TSE transmissibility was later also proven for other members of the TSE family: for Kuru, a meanwhile exterminated disease among aborigines in Papua New Guinea to chimpanzees [2] and the Creutzfeldt–Jakob disease (CJD) ([3], also to chimpanzees), whose authors first introduced the term "transmissible spongiform encephalopathy" [4]. Other members of the TSE family are summarized in Table 1.

In the 1960s it was taken for granted that TSEs were caused by a "slow virus", a term created by Bjorn Sigurdsson in 1954 [6], although no viral nucleic acid has been identified to date. Griffiths' theoretical work first suggested that the agent might be a protein [7]. In 1976, Gajdusek, a supporter of the slow virus theory, was awarded the Nobel prize for medicine within this scientific field. The first case of a new variant of CJD (vCJD), the clinical and neuropathological profiles of which were found to be noticeably different from sporadic CJD, was described 1996 in a patient younger than 40 years old in the UK. From 1995 to date, more than 150 suspected vCJD cases were reported in the United Kingdom, 110 of them were confirmed (http://www.cjd.ed.ac.uk/figures.htm). One year after the discovery of the variant CJD (vCJD), Hill et al. confirmed that BSE and vCJD were caused by the same prion strain, and concluded that the consumption of BSE-contaminated food is the most likely cause of vCJD in humans [8]. All TSE eventually result in death.

1.2. Prions: structure, function and the prion hypothesis

The causative agent of TSE is believed to be a protein, the so-called prion, a proteinaceous infectious particle that lacks agent-specific nucleic acid [9]. Over the past years, experimental evidence supporting this spectacular hypothesis has accumulated. Soto and colleagues, for example, generated infectious scrapie prions in vitro [10] and Kretzschmar and colleagues performed in vitro protein misfolding cyclic amplification (PMCA) experiments [11]. A major feature that

Table 1
Overview of the human and animal prion diseases (adapted from [5])

Host		Disease	Cause
Animal	Sheep/ Goat	Scrapie	vertical and horizontal infection in genetically susceptible sheep; oral transmission; sporadic
	Cattle	BSE (bovine spongiform encephalopathy)	Infection with prion-contaminated food; sporadic (?)
	Deer, Elk	CWD (chronic wasting disease)	Unclear, possibly similar to Scrapie
	Mink	TME (transmissible mink encephalopathy)	Infection with contaminated meat from sheep and cattle
	Cat	FSE (feline spongiform encephalopathy)	Infection with contaminated bovine tissue and food
Human		Kuru	Acquired through cannibalistic rituals
		CJD (Creutzfeldt–Jakob disease)	
		Familial	Inherited (mutation in the PrP gene)
		Sporadic	Spontaneous conversion of PrP^{C} into PrP^{Sc} (?)
		Iatrogenic	Acquired from contaminated instruments, dura mater grafts or growth hormone
		vCJD (variant CJD)	Acquired (infection by bovine prions)
		GSSS (Gerstmann–Sträussler–Scheinker syndrome)	Inherited (mutation in the PrP gene)
		FFI (fatal familial insomnia)	Inherited (mutation in the PrP gene)

distinguishes prions from viruses is that the non-pathogenic form of prions is encoded by a chromosomal gene [12], the PRNP gene, which is located on chromosome 20 in humans [13]. Despite an identical amino acid sequence, the prion protein can exist in different secondary (and tertiary) structures. PrP^{C}, the cellular prion protein, mainly but not exclusively expressed by neuronal cells, is high in α-helix (42%), whereas the misfolded or disease-associated form (Scrapie prion protein or PrP^{Sc}) shows a high amount of β-sheet structures (43%) and has less α-helix (30%) [14]. In Syrian hamsters, PrP^{C} is composed of 254 amino acids in its unprocessed form [15]. The signal sequence represented by amino acids 1–22 is truncated together with amino acids 232–254, resulting in the native prion protein. In comparison, the human PrP has 253 amino acids and shows 90% similarity to hamster PrP [16]. The two isoforms, PrP^{C} and PrP^{Sc}, not only differ in their secondary structure but also in their biochemical properties. PrP^{Sc} is insoluble in detergents, resistant against heat and only partially degradable by proteinase K. It forms fibrils and accumulates in the CNS, which is not the case for PrP^{C}.

The function of PrP is not fully understood yet. Recently, neuroprotective and antiapoptotic effects of the cellular prion protein were demonstrated [17]. PRNP knock-out mice ($PrP^{0/0}$) do not have a particular phenotype [18], but are completely resistant against prion inoculation and do not "replicate" the protein [19]. However, they exhibit some abnormalities in the synaptic physiology [20] and in circadian rhythms and sleep [21], as well as a reduced Cu^{2+} content (up to 50%) in membrane preparations [22] in comparison to wild type mice, arguing for a role of PrP in copper metabolism. In addition to copper ions [23–25], PrP^{C} also binds zinc, manganese, and nickel cations, although with lower affinities than for copper [26–28]. Most probably, the membrane-bound PrP^{C} seems to play a role in signal transduction, cell survival and differentiation. According to the "heterodimer" hypothesis [29,30] the cellular prion protein of a host is converted into PrP^{Sc} by partial unfolding into a transitional state designated PrP*; PrP* then refolds under the influence of PrP^{Sc}, resulting into a homodimer complex, possibly along with a hypothetical molecular chaperone. The newly generated PrP^{Sc} will then induce conversion of PrP^{C} in such an autocatalytic process.

1.3. The scrapie 263K hamster model

The Syrian hamster (*Mesocricetus auratus*) is a suitable model to study the pathology of the Scrapie strain 263K after oral uptake due to relatively short incubation time compared to sheep, goats or even mice [31] and the possibility to investigate large numbers of animals relatively easily. Attempts to transmit Scrapie to Syrian hamsters were started as early as 1965, when Zlotnik and Rennie transmitted mouse-passaged Scrapie to goats, sheep, rats, and hamsters [32]. In 1977, Kimberlin and Walker were the first to passage Scrapie strain 263K to *Mesocricetus auratus* [33]. The oral route of infection is presently viewed as the most epidemiologically relevant pathway for the natural transmission of Scrapie [34]. The nervous system of orally infected hamsters has been studied for the appearance of pathological prion protein [35]. The pathogenetic process was observed to begin in the spinal cord between vertebrae T4 and T9, and then show an antero- and retrograde spread with a rate of 0.8–1.0 mm/day [35]. These studies also revealed a possible alternative route of infection from the periphery to the brain via the spinal cord. Encouraged by this finding, a series of experiments was initiated with orally infected hamsters to unravel the route of the infectious agent to the brain [36,37], in which oral infection was achieved by feeding 3-week-old hamsters one-time with food pellets soaked with brain homogenate from terminally ill hamsters. After bypassing the gut, the misfolded PrP was detected in two distinct routes terminating in the CNS: The retrograde route starts from efferent, parasympathetic fibers and ends in the vagus nerve to the nucleus dorsalis nervi vagi (DMNV) and nucleus tracti solitarii (see schematic in Fig. 1) [36]. Both nuclei are located in the medulla oblongata, which is formed by the enlarged top of the spinal cord. The second route uses the efferent connections via pre-vertebral ganglia (ganglion coeliacum and ganglion mesentericum superius, CMGC) on nervus splanchnicus to the intermediolateral gray matter in the area between thoracic spinal cord segments T5–T12. From there the spread of PrP^{Sc} continues to the corresponding afferent dorsal root ganglia (nodules on a dorsal root that contain cell bodies of afferent nerve fibers), where the protein can first be detected 76 days post-infection in half of the examined hamsters [36,38,39].

1.4. FTIR microspectroscopy of biological tissue

An infrared spectrum of a biological sample is composed of characteristic absorption bands originating from all molecules it contains, such as proteins, lipids, nucleic acids, and others. Since the combination of all molecular parameters (structure, composition, and/or interactions) in a specific tissue structure, cell type, or part of a cell is unique, FTIR microspectroscopy, which provides fingerprint-like information, is capable of characterizing distinct tissue structures [40]. Over the past years, this has been shown for many types of tissues, mainly with the goal of developing efficient diagnostic procedures to detect tissue pathologies such as in the cervix [41,42], brain [43,44], colon [45–47], heart [48], and also individual normal and cancerous cells [49]. Brain tissue has been studied by vibrational spectroscopic methods for quite a long time for several reasons. One of them is the extraordinary high IR spectral contrast between white and gray matter of the brain (e.g. [50,51]), facilitating the development of spectral imaging methodologies on tissues [52]. Over the past decade it was shown that even small molecular differences (e.g., within gray matter brain structures and even sub-structures that are not easily identified by histology) can also be used for IR based differentiation in the cerebellum and the nuclei of the cranial nerves [44,53,54]. The second, and main reason for FTIR studies on brain tissue is that, together with Raman spectroscopy, it may be one of the only ways to elucidate the complex molecular background of some severe pathologies of the

central nervous system (CNS) in situ within the tissue. No labels, stains or dyes are required for FTIR microspectroscopy and it is a non-destructive, sensitive and fast tool. These are properties that cannot be achieved by other, either antibody/label- or purification-based methods.

Among the investigated pathologies in brain tissues are multiple sclerosis, where lesions in white matter (the myelin sheaths of neurons) were detected [51] and Alzheimer's disease, which is characterized by disease-specific, plaque-like protein accumulations, that can be detected by distinct changes in the amide I region of an IR spectrum [43,55]. This region of the vibrational spectrum gives information about the secondary structure of a protein in the investigated sample. Assignment of amide I band frequencies to secondary structures such as β-sheet or α-helix is given in Table 2.

2. Methods and approaches for studying scrapie-infected tissue by FTIR microspectroscopy

2.1. Animal experiments and sample preparation

All animal experiments were carried out in accordance with European and German legal and ethical regulations. Outbread Syrian hamsters were challenged orally with $1–3\times10^7$ 50% intracerebral lethal doses of scrapie strain 263K. Mock-infected hamsters of the same age were similarly fed with normal brain homogenate and served as control. The diseased hamsters were sacrificed by CO_2. The brain or the dorsal root ganglia attached to the thoracic spinal chord were removed and stored at −70 °C. Sequential cryo-sections were cut and mounted on IR transparent substrates (CaF_2 or BaF_2) (Korth Kristalle GmbH, Altenholz, Germany).

2.2. Conventional IR spectroscopic studies of brain tissue from scrapie infected hamsters

Infrared microspectroscopy was used to investigate the distribution and secondary structure of PrP in scrapie-infected and normal brain tissue. Three time points, 90 d.p.i., 120 d.p.i., and the terminal stage of the disease (150–160 d.p.i., varying between individuals) with four infected and four control animals for each time point were studied. Cryosections containing the nervus hypoglossus (HypN), the dorsal motor nucleus of the vagus nerve (DMNV), parts of the solitary tract nucleus (SolN) and the cerebellar nuclei were prepared on BaF_2 slides. For data acquisition, an IFS28/B FTIR spectrometer (Bruker, Ettingen, Germany) coupled to an IR microscope was used. The microscope was equipped with a mercury–cadmium–telluride detector, circular apertures, a 15x Cassegrain objective and a motorized stage. The OPUS 3.01 (Bruker) software was used to take spectra in transmission mode from the tissue sections. Absorbance spectra were acquired in the spectral range of 4000–700 cm^{-1} at 6 cm^{-1} spectral resolution, with Happ–Genzel apodization and a zero filling factor of 4 applied, yielding approximately one data point per wavenumber. The

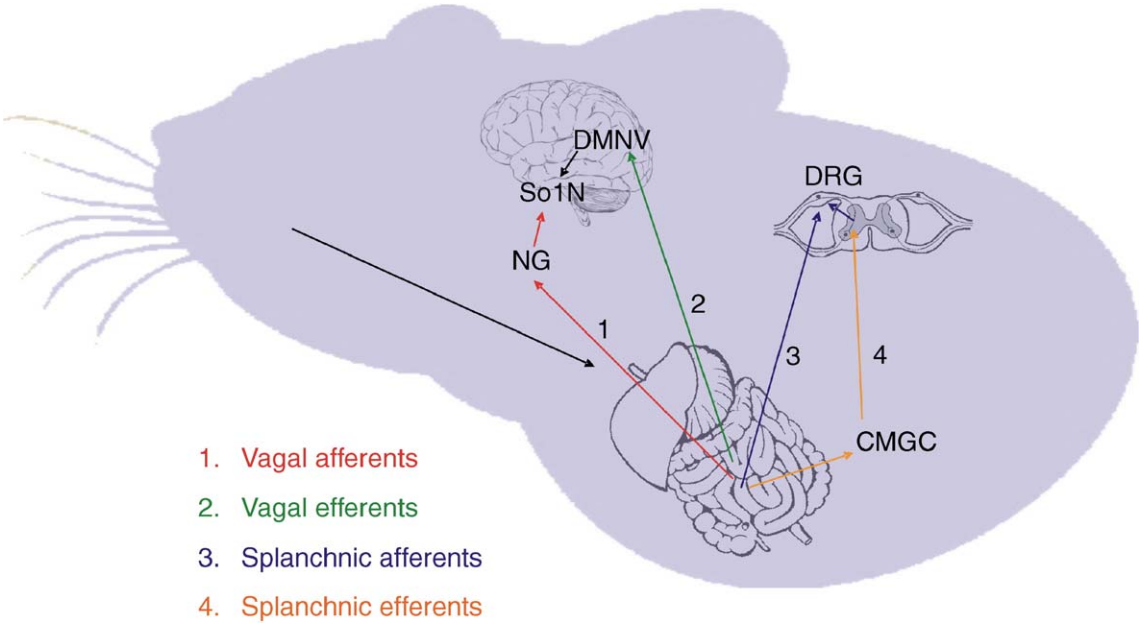

Fig. 1. Initial spread of the 263K agent after oral uptake. Circuitry has been simplified to show major routes only. The infectious agent reaches the CNS by spreading along either efferent (motor) or afferent (sensory) fibers of vagus or splanchnic nerves. Efferent fibers of the vagus nerve have their nerve cell bodies in the dorsal motor nucleus of the vagus nerve (DMNV) and synapse with neurons of the enteric nervous system in ganglia of the submucosal and myenteric plexuses in the wall of the alimentary canal. The nerve cells of vagus nerve afferent fibers are located in the nodosal ganglion (NG) and directly innervate the alimentary canal. These fibers run to the solitary tract nucleus (SolN), where they connect to interneurons projecting to the DMNV. The cell bodies of splanchnic nerve efferent fibers are located in the IML and interrelate to neurons of the coeliac mesenteriac ganglion complex (CMGC) that, in turn, innervate the gastrointestinal tract. Afferent fibers of the splanchnic nerve originate in the DRG, run through the CMGC, and directly innervate target organs such as the alimentary canal. Enteric and abdominal ganglia (CMCG) have an early involvement in pathogenesis. Adapted from [31].

Table 2
Assignment of absorption bands (cm^{-1}) to different secondary structures of proteins determined by measurements in H_2O (from: [56–58])

Amide I secondary structure assignments	
~1615–1625	Aggregated strands (intermolecular)
~1625–1640	β-sheet
~1650–1660	Disordered
~1650–1665	α-helix
Various bands between 1650 and 1690	Turns and loops
~1680–1695	Anti-parallel β-sheet

number of co-added interferograms per spectrum was set to 64 for "overview mapping" of larger tissue areas (4–6 mm^2) using 100 μm aperture diameter and to 512 scans for detailed mapping measurements using an aperture diameter of 50 μm.

2.3. Synchrotron FTIR imaging of dorsal root ganglion tissue of scrapie

It was found that not all prion proteins fold into the pathological form, even at the terminal stage of the disease. Therefore, the distribution of the PrP^{Sc} in the nervous system at different disease stages is of significance to understanding the pathological mechanism of scrapie. Infrared microspectroscopy, which combines infrared spectroscopy and microscopy, can be used to image the protein secondary structure of each pixel in a certain area of tissue. Since the nerve cells studied are of ~40–50 μm in diameter, and the PrP^{Sc} is not uniformly distributed throughout the cells, small IR beams (and thus small microscope apertures) are required to obtain sufficient spatial resolution. However, when using a conventional IR source apertures of 20 to 30 μm are needed to ensure sufficient light flux through the sample for good signal-to-noise. A Synchrotron infrared source is about 1000 times brighter than a conventional thermal (globar) source and therefore allows much smaller aperture setting (e.g. 6 × 6 μm) with acceptable signal-to-noise.

The FTIR imaging experiments were conducted at beamline U10B of the National Synchrotron Light Source, Brookhaven National Laboratory (Upton, NY). A Thermo Nicolet Magna 860 FTIR spectrometer, coupled to a Continuum IR microscope (ThermoNicolet, Madison, WI), was used with synchrotron light as the infrared source. The microscope was equipped with matching 32X Schwarzschild objectives, a motorized x–y mapping stage, an adjustable rectangular aperture, and a mercury cadmium telluride (MCT-A) detector. The aperture of the microscope was set to 10 × 10 μm. A pre-defined area was raster scanned with a step size of 4 μm using Omnic software (ThermoNicolet). At each point, an absorbance spectrum was recorded in transmission/absorbance mode. Each spectrum was collected in the mid-infrared spectral range (800–4000 cm^{-1}) with a spectral resolution of 8 cm^{-1} and 256 scans co-added. Happ–Genzel apodization and a zero-filling of level 2 were applied, resulting in approximately 1 data point per wavenumber.

2.4. Different spectroscopic regions analyzed in the scrapie studies

Three spectral regions were studied by FTIR microspectroscopy. The amide I band, located near 1650 cm^{-1}, is the most prominent absorption band of proteins. This absorption band is essentially due to >C═O stretching modes in the protein amide backbone. Differences in secondary structures (e.g.: α-helix, β-sheet) result in different peak positions and band shapes for amide I. In addition, the fingerprint region, containing contributions from carbohydrates and nucleic acids (1000–1300 cm^{-1}), and the lipid region (2800–3000 cm^{-1}) were analyzed to assess changes in cellular and membrane composition accompanying misfolding of prion protein in scrapie-infected nervous cells.

3. FTIR-based detection of pathological changes in scrapie-infected hamsters

The investigation of TSE in situ in nervous tissue is of basic interest, since the complex molecular background of the known morphological and ultrastructural changes in the course of the disease is far from being fully understood except for some selected parameters such as the PrP^{Sc} accumulation. In addition, the need for fast and efficient detection methods for prion diseases in the area of food safety gave the motivation to study prion-affected tissues by FTIR spectroscopy.

Early FTIR microspectroscopic experiments on orally scrapie-infected terminally diseased hamsters revealed molecular differences between the infected and control animals based on spectral changes detected in specific regions of the cerebellum (Stratum moleculare, Stratum ganglionare, Stratum granulosum and Substantia alba) [44]. It was observed that FTIR spectral differences between the various cerebellar histological structures were much larger than those between control and infected animals. It was therefore crucial to compare spectra of infected and uninfected material from exactly the same tissue substructures. Similar observations were made in FTIR-microspectroscopic studies of the medulla oblongata and of the cerebellar nuclei [54]. While clear spectral distinction between Scrapie-infected, homogenized medulla oblongata and pons tissue was possible for the terminal stage [44], it turned out to be difficult to differentiate in earlier (preclinical) stages. However, the comparison of spectra from specific nuclei in the medulla oblongata enabled identification of a disease-specific spectral pattern also in the pre-clinical stage [54]. It was demonstrated that the spectra need to be sorted according to the anatomical substructures before separating "diseased" and "non-diseased" spectral patterns [44]. It is only this method that avoids mixing up disease-specific and morphology-specific spectral differences.

To attain classification of brain-structure specific spectral patterns, univariate as well as multivariate analysis and image reconstruction techniques were used. In the case of the cerebellum, principal component analysis (PCA) was applied. Using this PCA approach, the four histologically defined layers *S. ganglionare*, *S. moleculare*, *S. granulosum* and *S. alba* could not only be separated to four distinct clusters but also into

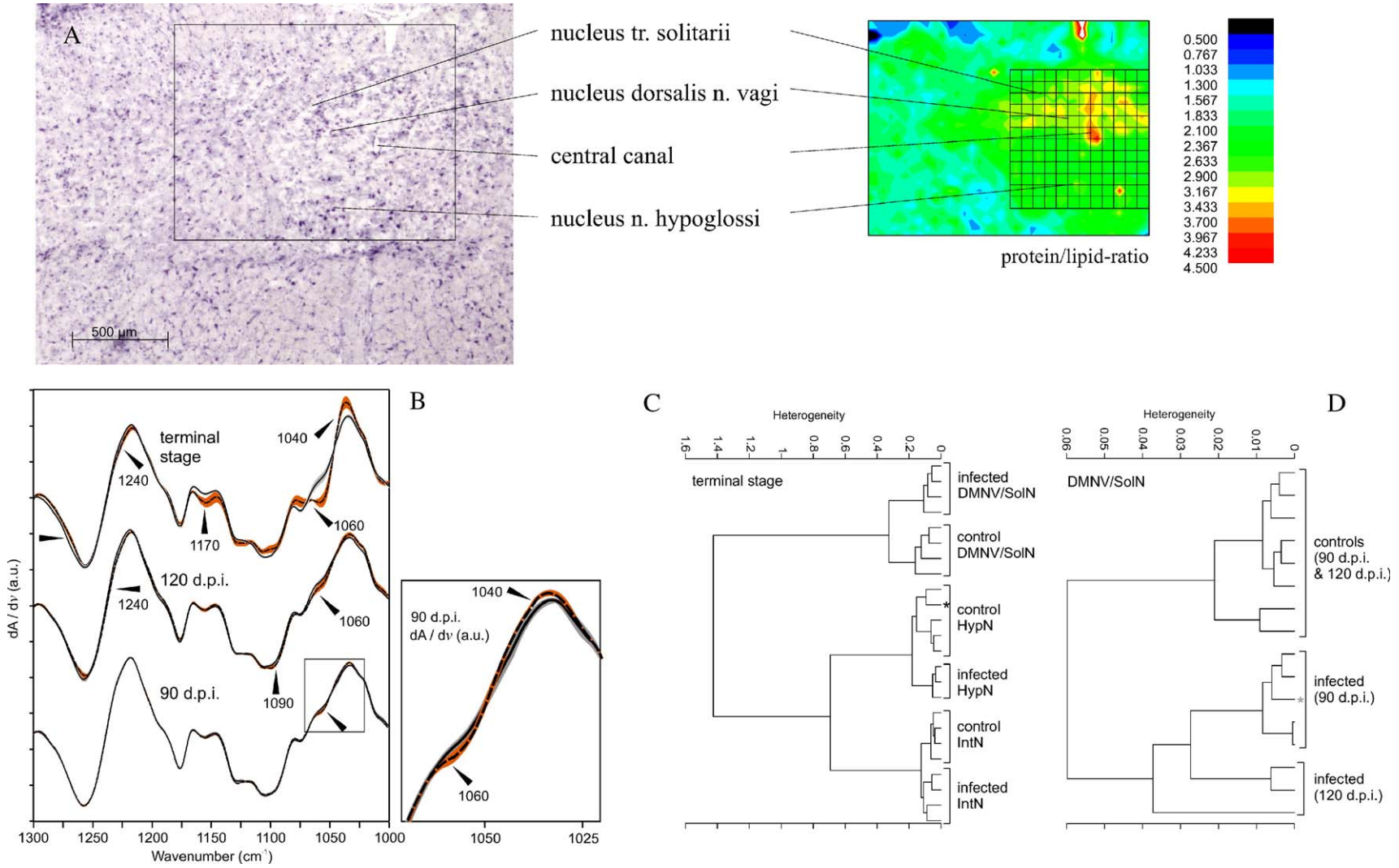

Fig. 2. (A) FTIR overview image based on the protein/lipid ratio calculated from the FTIR spectra (right) and visible micrograph of the cresyl fast violet stained adjacent tissue section (left; scale bar, 500 µm) for orientation in the medulla oblongata, containing the nuclei of the solitary tract, the DMNV and the nucleus of the HypN. The nuclei can be distinguished from the surrounding white matter by their high protein content shown as yellow and red areas in the right picture. The inset in the left photomicrograph indicates the tissue area investigated by IR imaging. The grids in the IR map show areas of detailed measurements that were performed for additional investigations. (B) Normalized first derivatives of average spectra of DMNV/SolN at three stages of the disease, each obtained from single spectra of four scrapie-infected hamsters (dashed lines) and four control hamsters (solid lines) with their standard deviations (dark, infected; light, normal controls) displayed over the frequency range 1000–1300 cm^{-1}. Arrowheads indicate differences between spectra. The inset displays the spectral region containing subtle differences between the averages at 90 d.p.i. (C) Cluster analyses of spectra of the DMNV/SolN, HypN, and IntN of four terminally diseased and four control animals using the spectral information between 950 and 1480 cm^{-1}. The spectrum of the HypN of one of the infected hamsters was grouped with the controls (asterisk). (D) Cluster analysis of spectra from the DMNV/SolN of eight infected hamsters (four 120 d.p.i. and four 90 d.p.i.) and the corresponding eight controls based on the spectral information between 1025 and 1050 cm^{-1}. All first-derivative spectra were normalized over the frequency range 1000–1300 cm^{-1}. One infected individual at 120 d.p.i. appears in the 90 d.p.i. group (asterisk). Adapted from [54]. Copyright 2002 by the Society für Neuroscience.

substructures that were not distinguishable by common dyeing methods such as cresyl violet or hematoxylin/eosin staining [44]. In a second step, hierarchical cluster analysis was performed on single pixel spectra of the latter three histological structures from scrapie-infected and control hamsters revealing a clear separation between spectra of infected and uninfected animals. In analyzing the spectra, the protein/lipid ratio turned out to be useful to distinguish spectra of the nuclei of the cranial nerves from the surrounding tissue (high protein content of the nuclei and high lipid content of the adjacent areas, see Fig. 2A) in the medulla oblongata. The protein/lipid ratio, however, was shown to be able to distinguish only between the gray and white matter in hippocampus [59]. The DMNV and solitary tract nucleus could further be separated from the hypoglossal nucleus in a cluster analysis-based IR imaging procedure [54]. Spectral changes due to the scrapie infection vary in extent and quality for the different brain structures. In the cerebellum, to give an example, alterations could be detected in the spectral region between 2800 and 3050 cm^{-1} (dominated by absorption bands of the asymmetric and symmetric C–H stretching vibrations of $>CH_2$ and $>CH_3$ methylene groups) and in the fingerprint region between 1000 and 1300 cm^{-1}. Changes in the CH-stretching region led to the assumption that an altered protein composition of the membranous system influenced the membrane state-of-order via lipid–protein-interactions. Changes in the fingerprint region (1000–1300 cm^{-1}) were not only observed in the area of the cerebellum, but also in the nuclei of the medulla oblongata [54]. In fact, the earliest spectral changes that were observed in a longitudinal study of the disease progression in this part of the brain occurred 90 days post-infection in the DMNV. These alterations were observed in the spectral region between 1040 and 1060 cm^{-1} (see Fig. 2D) and were shown to be indicative of an altered composition and/or structure of carbohydrates (sugar moieties of nucleic acids or changed content of metabolic sugar molecules in the cell such as glucose). The early stage of the disease has been characterized by microvacuolation [60], membrane proliferation, structural and functional damage of mitochondria [61] and DNA decomposition during apoptosis and/or a changed RNA content as the result of up- or down-regulation of genes [62]. By cluster analyses on DMNV spectra from diseased and control animals at 90 and 120 days postinfection, respectively, spectra from infected animals could be clearly separated from controls (see Fig. 2C). Worth mentioning is the fact that 90 d.p.i. spectra and 120 d.p.i. spectra did not form two distinct classes, indicating that progression of molecular changes is individually variable. The fact that the earliest spectral changes were reported to occur in the DMNV is in accordance with earlier pathogenesis studies which used immunohistology of the misfolded PrP^{Sc} as the disease marker [38].

Interestingly, although the disease is characterized by the accumulation of a misfolded protein, no statistically relevant differences in the amide I region were found in any of the data sets acquired with standard FTIR microspectroscopic microscopes using conventional globar sources and single-element detectors [54,59]. This observation holds true even for anatomical structures known to show early and intense PrP^{Sc} accumulations in the 263K hamster model (DMNV). As shown in Fig. 3, the local protein concentration was too low to be detected at the given spatial resolution. PrP^{Sc} accounts for less than 0.1% of all proteins in the diseased brain tissue in the terminal stage [35]. An FTIR spectrum is always the sum of

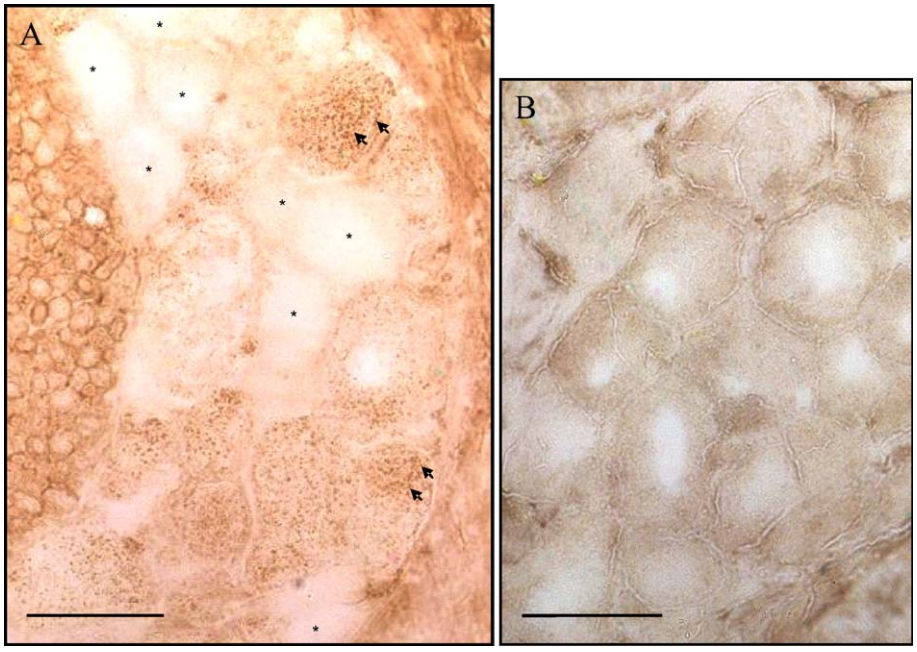

Fig. 3. Sections of dorsal root ganglia from an infected (A) and a control (B) animal stained with the PrP specific antibody 3F4. Arrows indicate areas with a high PrP^{Sc} deposition. The pathological prion protein can be detected as dark brown dots in most of the cells but not all (see asterisk marked cells). Since 3F4 stains both PrP^{Sc} and PrP^{C}, B shows a 3F4 stained control slide as an example of the PrP^{C} distribution (brown color). (scale bars, 50 μm).

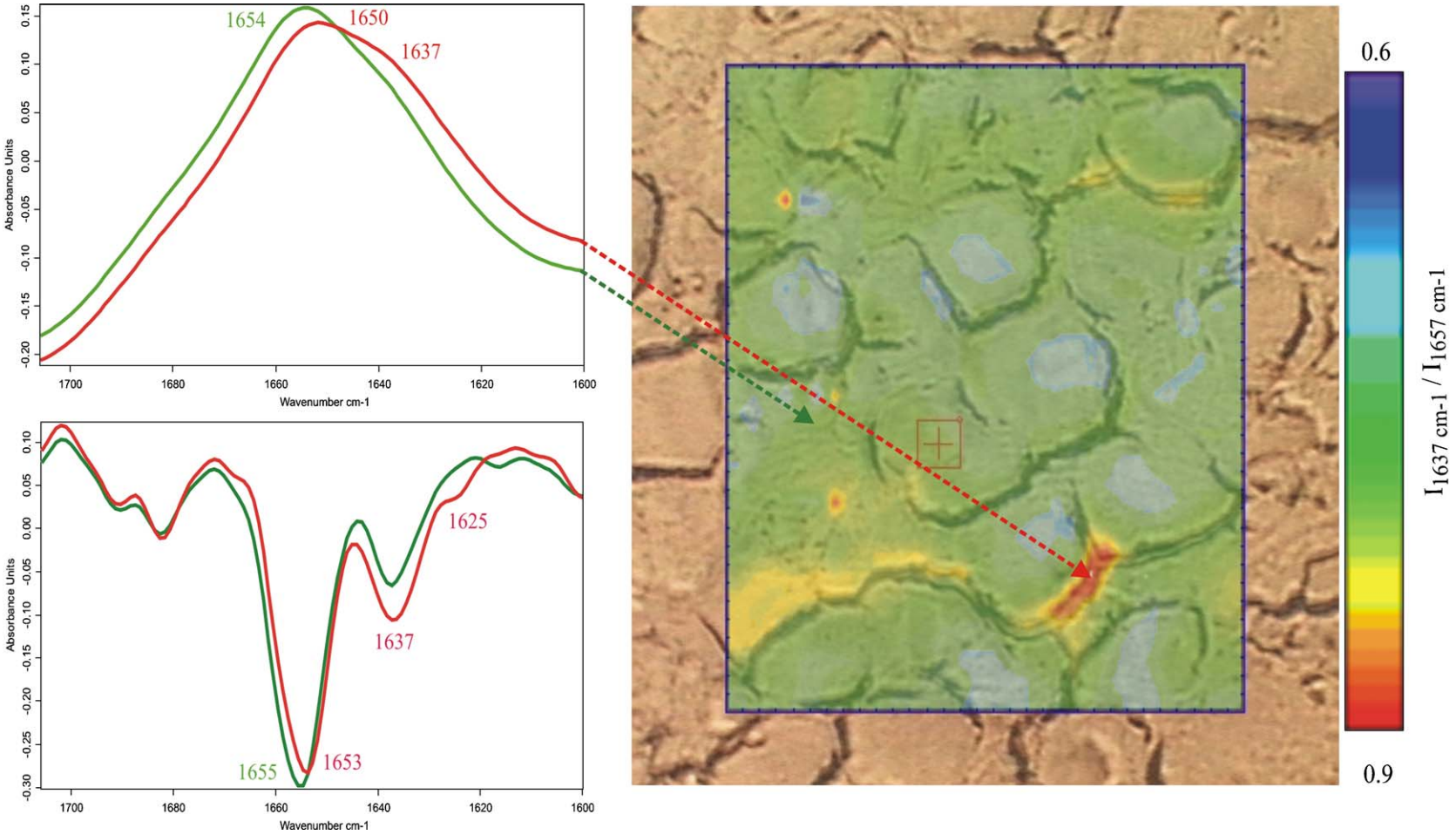

Fig. 4. IR map and spectra of a dorsal root ganglion from a terminally diseased hamster. Right picture shows a photomicrograph (scale bar, 50 μm) with the IR mapped area overlaid. The ratio of the β-sheet to α-helical intensities calculated from the absorbance at 1637 cm^{-1} and 1657 cm^{-1}, respectively, is shown as a function of pixel location. Red and yellow indicate areas with a relatively higher β-sheet content than spectra from green and blue areas. Examples of amide I band shapes of spectra from areas with relatively higher (red) and lower (green) β-sheet content are shown on the upper left (original spectra, normalized between 1400 and 1800 cm^{-1}) and lower left side (corresponding second derivative spectra).

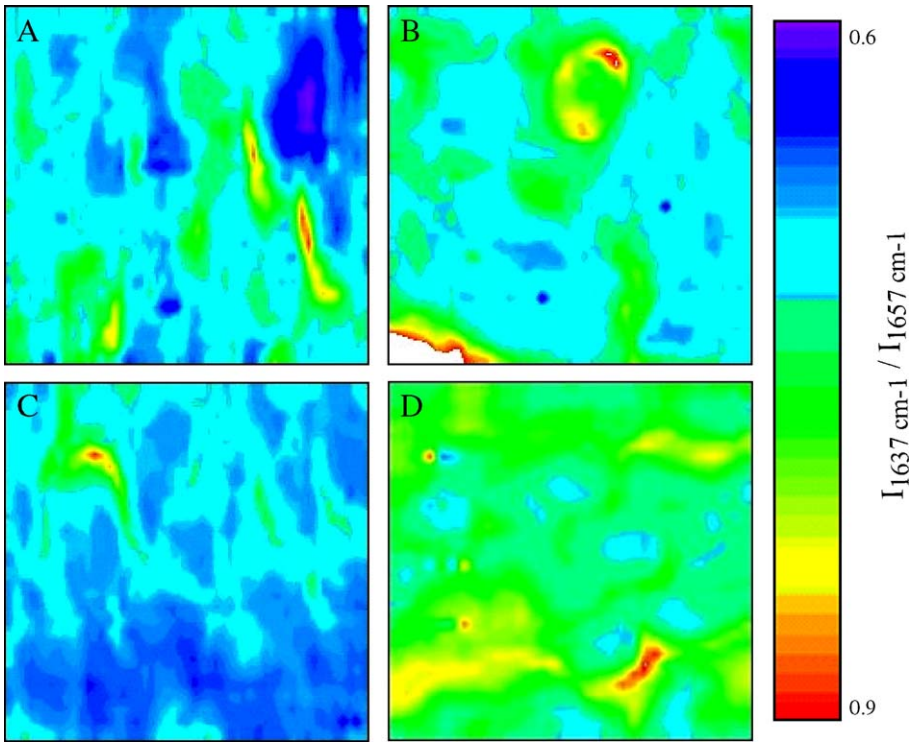

Fig. 5. IR images of one infected and one control animal at 130 d.p.i. and the terminal stage of disease, respectively. Images graphically present the ratio of β-sheet to α-helix content calculated as $I_{1637\ cm-1}/I_{1657\ cm-1}$ as a function of pixel location. (A) Control animal at 130 d.p.i. (B) 263K infected animal at 130 d.p.i. (C) Control animal, terminal stage of disease. (D) 263K infected animal, terminal stage of disease. An overall more green, yellow and red coloring can be seen by comparing the corresponding control and infected samples (A versus B and C versus D; controls to infected at 130 d.p.i. and terminal stage, respectively) but also by comparing B and D (infected animal at 130 d.p.i. to infected animal at terminal stage), clearly showing the progression of PrP^{Sc} deposition during pathogenesis.

individual spectral components from the structures under investigation. Thus, the acquisition of high quality FTIR microspectra from the smallest possible sample volume is indispensable for detection of small-sized accumulations such as the protein aggregate, PrP^{Sc}, in the brain. As has been illustrated recently, this "optical dilution effect" makes it

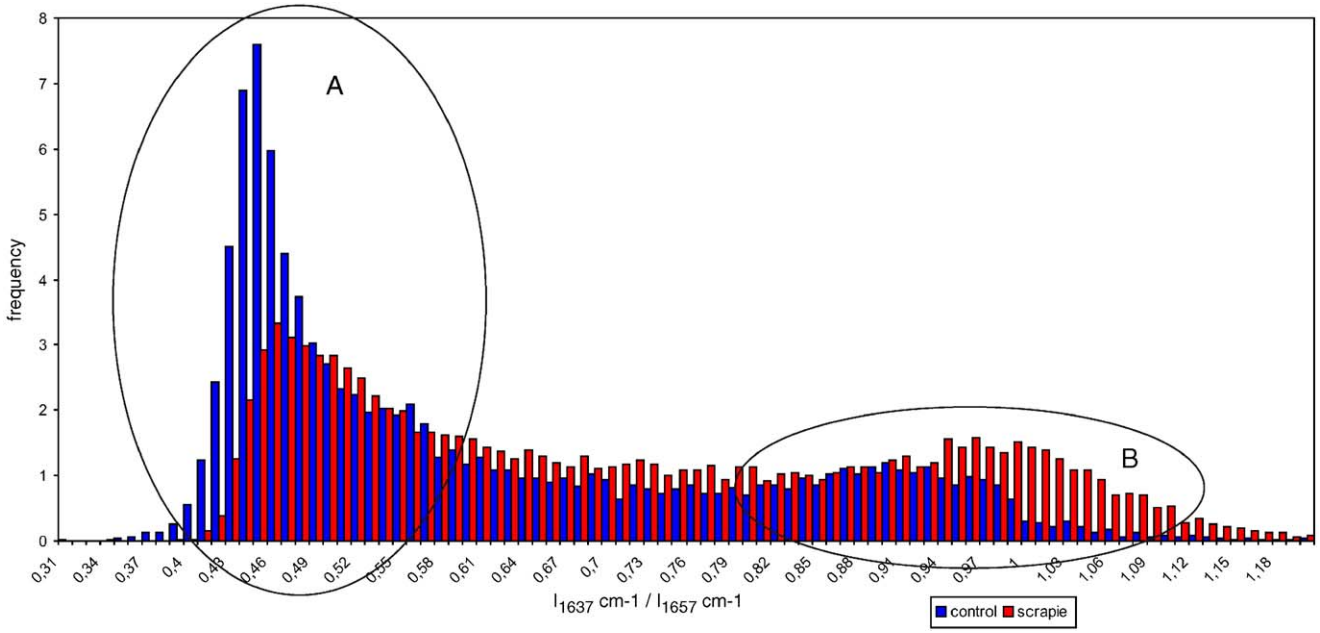

Fig. 6. Histogram of relative β-sheet content calculated from 11025 spectra of control (blue) and 18422 spectra of terminal diseased (red) hamsters. *x* axis indicates the proportion of β-sheet to α-helix as calculated from the IR spectra, the relative number of spectra is given on the *y* axis. The graph represents two distributions with two maxima each; remarkable differences are indicated by areas A and B. While the two distributions appear similar between 0.5 and 0.94, significantly more spectra from diseased hamsters exhibit an elevated β-sheet (see area B) and a lower α-helix content (see area A), respectively.

impossible to detect microdisperse PrP^{Sc} aggregates even with apertures as large as $30 \times 30\ \mu m^2$ [63].

4. FTIR microspectroscopy of dorsal root ganglia utilizing a synchrotron IR light source

In a recent pilot study, spectra from dorsal root ganglia of 263K hamsters were acquired using a synchrotron, which provides a spatial resolution approaching the diffraction limit of mid-infrared light [64]. Thirty-one neurons from infected and thirty-two neurons from control hamster were investigated, respectively. Although the diffraction limit of IR light is ~6 μm at 1650 cm^{-1}, which is still bigger than the size of typical PrP^{Sc} aggregates in 263K, differences associated with PrP^{Sc} deposition could be detected in the amide I region with aperture sizes of 10 μm [64]. Results showed that the peak at around 1657 cm^{-1}, associated with α-helical protein structures, decreased and shifted to lower frequency in spectra from infected animals, and the peak at ~1637 cm^{-1} increased. In some spectra from infected hamsters, an additional peak at around 1631 cm^{-1} also appeared. This argues for a higher β-sheet and lower α-helix content of the proteins in the investigated areas. Similarly small sampling volumes were reported in an experiment using a focal plane array detector to study the hippocampus of 263K-infected hamsters and yielded some spectra with a changed amide I contour that could indicate diffuse protein deposits [59].

More recent synchrotron FTIR spectroscopic studies supporting the results of the initial study have been extended to a larger number of animals [48]. To date, more than 120 cells from 5 263k-infected animals and 105 cells from 4 control animals have been measured, such that about 18422 and 11025 spectra were collected from diseased and control hamsters, respectively. Fig. 4 shows a typical example from a scrapie-infected dorsal root ganglion. The rectangle in the photomicrograph indicates the investigated sample area overlaid with the corresponding chemical map, which was calculated by the ratio of the intensities from baseline corrected original absorbance spectra at peak positions 1637 cm^{-1} and 1657 cm^{-1} (I_{1637}/I_{1657}), respectively. This chemical image shows predominantly green regions, which indicate that the majority of spectra have a I_{1637}/I_{1657} ratio around 0.75; and some yellow and red areas indicating regions of elevated β-sheet located close to the cell membrane. The spatial resolution of the technique is not high enough to determine whether these regions are intra- or extracellular. Representative spectra taken from green and red areas are shown on the left as original absorbance (top) and as second derivative spectra (bottom). The peak maximum of the amide I band in the original spectra shows a downshift from 1654 cm^{-1} to 1650 cm^{-1} in spectra from areas with decreased α-helical structures and additionally a shoulder around 1637 cm^{-1}, which corresponds to β-sheet. Plotting these spectra as second derivatives, an additional peak at 1625 cm^{-1} and a small downshift from 1655 cm^{-1} to 1653 cm^{-1} can be observed in some of the spectra.

In Fig. 5, representative univariate maps calculated by I_{1637}/I_{1657} are shown for one map of a control animal at 130 d.p.i. (Fig. 5A), one infected animal at 130 d.p.i. (Fig. 5B), one control animal at terminal stage (Fig. 5C) and one infected animal at terminal stage (Fig. 5D). Comparison of tissue samples from control and diseased animals at the same time points as well as comparison of spectra from diseased animals at different time points show remarkable differences, indicating progression of PrP^{Sc} deposition during pathogenesis. The spectra with altered amide I band, i.e. downshifted peak maxima in control maps can be explained by the fact that proteins in a normal tissue have a wide variety of structures, so some may show similar amide I band shapes as spectra obtained from areas with a PrP^{Sc} deposition. But a comparison with immunostained adjacent slides excluded the presence of misfolded prion protein in control tissue.

The histogram shown in Fig. 6 illustrates the relative β-sheet content calculated from 11025 control spectra and 18422 diseased spectra measured with synchrotron FTIR microspectroscopy. The x-axis indicates the proportion of β-sheet to α-helix in the investigated proteins, while the relative number of spectra is given by the y-axis. Regarding the distribution of the β-sheet to α-helix ratio taken from control animals (blue bars) it can be concluded that the majority of investigated proteins is high in α-helix (see area A) and only a minority is high in β-sheet (see area B). This can be explained by normal variations among proteins in neuronal tissue. In contrast, the β-sheet to α-helix ratio of proteins in scrapie-infected tissue (red bars) shows that significantly less spectra are high in α-helix (see area A) and exhibit an elevated β-sheet content instead (see area B). Based on these FTIR microspectroscopic findings, and by comparison with immunostained adjacent sections, we concluded that the spectral signals indicating elevated β-sheet content are due to PrP^{Sc} deposition.

5. Concluding remarks and outlook

FTIR microspectroscopy, one of the few spectroscopic techniques that can detect changes in many different biomolecules simultaneously and in situ, has proven to be a useful tool for the detection of disease-specific molecular changes directly in the tissue, shedding new light on prion pathogenesis. IR microspectroscopic imaging data at a spatial resolution of about 40 μm can be used to identify distinct histological structures in nervous tissues. Based on these structure specific spectra distinct differences between prion-infected and non-infected tissue can be elucidated even at pre-clinical stages of the disease. At a spatial resolution close to the diffraction limit for IR (~2–10 μm) specific features appear in some of the spectra of scrapie-infected neurons at 1637 cm^{-1} and 1631 cm^{-1}, typical of a β-sheet secondary structures, which can be used to characterize the misfolded prion protein in situ. To learn more about prion structural biology in situ, the FTIR-microspetroscopic approach has recently been combined with x-ray fluorescence microprobe, where the presence of distinct metal ions are correlated with the presence of PrP^{Sc} features [48]. To develop further IR-based screening or diagnostic methods, other organs and body fluids should also be investigated for their potential to serve as possible analytical samples. The successful identification of TSE from sera of BSE infected cattle is a first

promising result on the way towards spectroscopy-based TSE detection [65].

Acknowledgements

The authors like to thank Marion Joncic and Kristin Kampf for skilful technical assistance with the animal experiments.

References

[1] R.L. Chandler, Encephalopathy in mice produced by inoculation with scrapie brain material, Lancet 1 (1961) 1378–1379.
[2] D.C. Gajdusek, C.J. Gibbs, M. Alpers, Experimental transmission of a Kuru-like syndrome to chimpanzees, Nature 209 (1966) 794–796.
[3] C.J. Gibbs Jr., D.C. Gajdusek, D.M. Asher, M.P. Alpers, E. Beck, P.M. Daniel, W.B. Matthews, Creutzfeldt–Jakob disease (spongiform encephalopathy): transmission to the chimpanzee, Science 161 (1968) 388–389.
[4] K. Ravilochan, K.L. Tyler, Human transmissible neurodegenerative diseases (prion diseases), Semin. Neurol. 12 (1992) 178–192.
[5] M. Nunziante, The subcellular trafficking of the prion protein: Characterisation of the function of the PrPc N-terminus, Dissertation (2003).
[6] B. Sigurdsson, Rida, a chronic encephalitis of sheep. With general remarks on infections which develop slowly and some of their special characteristics. Brit. Vet. J. 110 (1954) 341–354.
[7] J.S. Griffith, Self-replication and scrapie, Nature 215 (1967) 1043–1044.
[8] A.F. Hill, M. Desbruslais, S. Joiner, K.C. Sidle, I. Gowland, J. Collinge, L.J. Doey, P. Lantos, The same prion strain causes vCJD and BSE. Nature 389 (1997) 448-450, 526.
[9] S.B. Prusiner, Prion diseases and the BSE crisis, Science 278 (1997) 245–251.
[10] J. Castilla, P. Saa, C. Hetz, C. Soto, In vitro generation of infectious scrapie prions, Cell 121 (2005) 195–206.
[11] J. Bieschke, P. Weber, N. Sarafoff, M. Beekes, A. Giese, H. Kretzschmar, Autocatalytic self-propagation of misfolded prion protein, Proc. Natl. Acad. Sci. U. S. A. 101 (2004) 12207–12211.
[12] S.B. Prusiner, Prions, Proc. Natl. Acad. Sci. U. S. A. 95 (1998) 13363–13383.
[13] N.K. Robakis, E.A. Devine-Gage, E.C. Jenkins, R.J. Kascsak, W.T. Brown, M.S. Krawczun, W.P. Silverman, Localization of a human gene homologous to the PrP gene on the p arm of chromosome 20 and detection of PrP-related antigens in normal human brain, Biochem. Biophys. Res. Commun. 140 (1986) 758–765.
[14] K.M. Pan, M. Baldwin, J. Nguyen, M. Gasset, A. Serban, D. Groth, I. Mehlhorn, Z. Huang, R.J. Fletterick, F.E. Cohen, et al., Conversion of alpha-helices into beta-sheets features in the formation of the scrapie prion proteins, Proc. Natl. Acad. Sci. U. S. A. 90 (1993) 10962–10966.
[15] K. Basler, B. Oesch, M. Scott, D. Westaway, M. Walchli, D.F. Groth, M.P. McKinley, S.B. Prusiner, C. Weissmann, Scrapie and cellular PrP isoforms are encoded by the same chromosomal gene, Cell 46 (1986) 417–428.
[16] H.A. Kretzschmar, L.E. Stowring, D. Westaway, W.H. Stubblebine, S.B. Prusiner, S.J. Dearmond, Molecular cloning of a human prion protein cDNA, DNA 5 (1986) 315–324.
[17] X. Roucou, P.N. Giannopoulos, Y. Zhang, J. Jodoin, C.G. Goodyer, A. LeBlanc, Cellular prion protein inhibits proapoptotic Bax conformational change in human neurons and in breast carcinoma MCF-7 cells, Cell Death Differ. 12 (2005) 783–795.
[18] H. Bueler, M. Fischer, Y. Lang, H. Bluethmann, H.P. Lipp, S.J. DeArmond, S.B. Prusiner, M. Aguet, C. Weissmann, Normal development and behaviour of mice lacking the neuronal cell-surface PrP protein, Nature 356 (1992) 577–582.
[19] H. Bueler, A. Aguzzi, A. Sailer, R.A. Greiner, P. Autenried, M. Aguet, C. Weissmann, Mice devoid of PrP are resistant to scrapie, Cell 73 (1993) 1339–13347.
[20] J. Collinge, M.A. Whittington, K.C. Sidle, C.J. Smith, M.S. Palmer, A.R. Clarke, J.G. Jefferys, Prion protein is necessary for normal synaptic function, Nature 370 (1994) 295–297.
[21] I. Tobler, S.E. Gaus, T. Deboer, P. Achermann, M. Fischer, T. Rulicke, M. Moser, B. Oesch, P.A. McBride, J.C. Manson, Altered circadian activity rhythms and sleep in mice devoid of prion protein, Nature 380 (1996) 639–642.
[22] D.R. Brown, K. Qin, J.W. Herms, A. Madlung, J. Manson, R. Strome, P.E. Fraser, T. Kruck, A. von Bohlen, W. Schulz-Schaeffer, A. Giese, D. Westaway, H. Kretzschmar, The cellular prion protein binds copper in vivo, Nature 390 (1997) 684–687.
[23] D.R. Brown, B. Schmidt, H.A. Kretzschmar, Effects of copper on survival of prion protein knockout neurons and glia, J. Neurochem. 70 (1998) 1686–1693.
[24] P.C. Pauly, D.A. Harris, Copper stimulates endocytosis of the prion protein, J. Biol. Chem. 273 (1998) 33107–33110.
[25] J.H. Viles, F.E. Cohen, S.B. Prusiner, D.B. Goodin, P.E. Wright, H.J. Dyson, Copper binding to the prion protein: structural implications of four identical cooperative binding sites, Proc. Natl. Acad. Sci. U. S. A. 96 (1999) 2042–2047.
[26] K.M. Pan, N. Stahl, S.B. Prusiner, Purification and properties of the cellular prion protein from Syrian hamster brain, Protein Sci. 1 (1992) 1343–1352.
[27] D.R. Brown, F. Hafiz, L.L. Glasssmith, B.S. Wong, I.M. Jones, C. Clive, S.J. Haswell, Consequences of manganese replacement of copper for prion protein function and proteinase resistance, EMBO J. 19 (2000) 1180–1186.
[28] G.S. Jackson, I. Murray, L.L. Hosszu, N. Gibbs, J.P. Waltho, A.R. Clarke, J. Collinge, Location and properties of metal-binding sites on the human prion protein, Proc. Natl. Acad. Sci. U. S. A. 98 (2001) 8531–8535.
[29] S.B. Prusiner, Novel proteinaceous infectious particles cause scrapie, Science 216 (1982) 136–144.
[30] F.E. Cohen, K.M. Pan, Z. Huang, M. Baldwin, R.J. Fletterick, S.B. Prusiner, Structural clues to prion replication, Science 264 (1994) 530–531.
[31] M. Baier, S. Norley, J. Schultz, M. Burwinkel, A. Schwarz, C. Riemer, Prion diseases: infectious and lethal doses following oral challenge, J. Gen. Virol. 84 (2003) 1927–1929.
[32] I. Zlotnik, J.C. Rennie, Experimental transmission of mouse passaged scrapie to goats, sheep, rats and hamsters, J. Comp. Pathol. 75 (1965) 147–157.
[33] R.H. Kimberlin, C.A. Walker, Characteristics of a short incubation model of scrapie in the golden hamster, J. Gen. Virol. 34 (1977) 295–304.
[34] H. Diringer, M. Beekes, U. Oberdieck, The nature of the scrapie agent: the virus theory, Ann. N. Y. Acad. Sci. 724 (1994) 246–258.
[35] M. Beekes, E. Baldauf, H. Diringer, Sequential appearance and accumulation of pathognomonic markers in the central nervous system of hamsters orally infected with scrapie, J. Gen. Virol. 77 (Pt 8) (1996) 1925–1934.
[36] M. Beekes, P.A. McBride, E. Baldauf, Cerebral targeting indicates vagal spread of infection in hamsters fed with scrapie, J. Gen. Virol. 79 (Pt 3) (1998) 601–607.
[37] E. Baldauf, M. Beekes, H. Diringer, Evidence for an alternative direct route of access for the scrapie agent to the brain bypassing the spinal cord, J. Gen. Virol. 78 (Pt 5) (1997) 1187–1197.
[38] P.A. McBride, W.J. Schulz-Schaeffer, M. Donaldson, M. Bruce, H. Diringer, H.A. Kretzschmar, M. Beekes, Early spread of scrapie from the gastrointestinal tract to the central nervous system involves autonomic fibers of the splanchnic and vagus nerves, J. Virol. 75 (2001) 9320–9327.
[39] P.A. McBride, M. Beekes, Pathological PrP is abundant in sympathetic and sensory ganglia of hamsters fed with scrapie, Neurosci. Lett. 265 (1999) 135–138.
[40] D.L. Wetzel, S.M. LeVine, Imaging molecular chemistry with infrared microscopy, Science 285 (1999) 1224–1225.
[41] M.J. Romeo, Influence of benign cellular changes in diagnosis of cervical cancer using IR microspectroscopy, Biopolymers 67 (2002) 362–366.
[42] L. Chiriboga, P. Xie, H. Yee, V. Vigorita, D. Zarou, D. Zakim, M. Diem, Infrared spectroscopy of human tissue. I. Differentiation and maturation of epithelial cells in the human cervix, Biospectroscopy 4 (1998) 47–53.

[43] L.P. Choo, D.L. Wetzel, W.C. Halliday, M. Jackson, S.M. LeVine, H.H. Mantsch, In situ characterization of beta-amyloid in Alzheimer's diseased tissue by synchrotron Fourier transform infrared microspectroscopy, Biophys. J. 71 (1996) 1672–1679.
[44] J. Kneipp, P. Lasch, E. Baldauf, M. Beekes, D. Naumann, Detection of pathological molecular alterations in scrapie-infected hamster brain by Fourier transform infrared (FT-IR) spectroscopy, Biochim. Biophys. Acta 1501 (2000) 189–199.
[45] P. Lasch, W. Haensch, D. Naumann, M. Diem, Imaging of colorectal adenocarcinoma using FT-IR microspectroscopy and cluster analysis, Biochim. Biophys. Acta 1688 (2004) 176–186.
[46] P. Lasch, D. Naumann, FT-IR microspectroscopic imaging of human carcinoma thin sections based on pattern recognition techniques, Cell. Mol. Biol. (Noisy-le-grand) 44 (1998) 189–202.
[47] L. Zhang, G.W. Small, A.S. Haka, L.H. Kidder, E.N. Lewis, Classification of Fourier transform infrared microscopic imaging data of human breast cells by cluster analysis and artificial neural networks, Appl. Spectrosc. 57 (2003) 14–22.
[48] Q. Wang, A. Kretlow, M. Beekes, D. Naumann, L. Miller, In situ characterization of prion protein structure and metal accumulation in scrapie-infected cells by synchrotron infrared and X-ray imaging, J. Vib. Spec. 38 (2005) 61–69.
[49] M. Diem, L. Chiriboga, P. Lasch, A. Pacifico, IR spectra and IR spectral maps of individual normal and cancerous cells, Biopolymers 67 (2002) 349–353.
[50] S.M. LeVine, D.L.B. Wetzel, Analysis of brain tissue by FT-IR microspectroscopy, Appl. Spectrosc. Rev. 28 (1993) 385–412.
[51] L.P. Choo, M. Jackson, W.C. Halliday, H.H. Mantsch, Infrared spectroscopic characterisation of multiple sclerosis plaques in the human central nervous system, Biochim. Biophys. Acta 1182 (1993) 333–337.
[52] E.N. Lewis, A.M. Gorbach, C. Marcott, I.W. Levin, High-fidelity Fourier transform infrared spectroscopic imaging of primate brain tissue, Appl. Spectrosc. Rev. 50 (1996) 263–269.
[53] D.S. Lester, L.H. Kidder, I.W. Levin, E.N. Lewis, Infrared microspectroscopic imaging of the cerebellum of normal and cytarabine treated rats, Cell. Mol. Biol. (Noisy-le-grand) 44 (1998) 29–38.
[54] J. Kneipp, M. Beekes, P. Lasch, D. Naumann, Molecular changes of preclinical scrapie can be detected by infrared spectroscopy, J. Neurosci. 22 (2002) 2989–2997.
[55] L.M. Miller, Q. Wang, T.P. Telivala, R.J. Smith, A. Lanzirotti, J. Miklossy, Synchrotron-based infrared and X-ray imaging shows focalized accumulation of Cu and Zn co-localized with β-amyloid deposits in Alzheimer's disease, J. Struct. Biol. 115 (2006) 30–37.
[56] A. Dong, P. Huang, W.S. Caughey, Protein secondary structures in water from second-derivative amide I infrared spectra, Biochemistry 29 (1990) 3303–3308.
[57] A. Barth, C. Zscherp, What vibrations tell us about proteins? Q. Rev. Biophys. 35 (2002) 369–430.
[58] H. Fabian, W. Mäntele. Vol. 5, pp. 3399–3425, John Wiley & Sons 2002.
[59] J. Dubois, R. Baydack, E. McKenzie, T. Booth, M. Jackson, Scrapie infection investigated by magnetic resonance imaging and Fourier transform infrared microscopy, J. Vib. Spec. 32 (2003) 95–105.
[60] R.F. Marsh, R.H. Kimberlin, Comparison of scrapie and transmissible mink encephalopathy in hamsters: II. Clinical signs, pathology, and pathogenesis, J. Infect. Dis. 131 (1975) 104–110.
[61] S.I. Choi, W.K. Ju, E.K. Choi, J. Kim, H.Z. Lea, R.I. Carp, H.M. Wisniewski, Y.S. Kim, Mitochondrial dysfunction induced by oxidative stress in the brains of hamsters infected with the 263K scrapie agent, Acta Neuropathol. (Berl) 96 (1998) 279–286.
[62] C. Riemer, I. Queck, D. Simon, R. Kurth, M. Baier, Identification of upregulated genes in scrapie-infected brain tissue, J. Virol. 74 (2000) 10245–10248.
[63] J. Kneipp, L.M. Miller, S. Spassov, F. Sokolowski, P. Lasch, M. Beekes, D. Naumann, Scrapie-infected cells, isolated prions, and recombinant prion protein: a comparative study, Biopolymers 74 (2004) 163–167.
[64] J. Kneipp, L.M. Miller, M. Joncic, M. Kittel, P. Lasch, M. Beekes, D. Naumann, In situ identification of protein structural changes in prion-infected tissue, Biochim. Biophys. Acta 1639 (2003) 152–158.
[65] P. Lasch, J. Schmitt, M. Beekes, T. Udelhoven, M. Eiden, H. Fabian, W. Petrich, D. Naumann, Antemortem identification of bovine spongiform encephalopathy from serum using infrared spectroscopy, Anal. Chem. 75 (2003) 6673–6678.